The effect of consistency on the shear rheology of micro- and nanofibrillated cellulose suspensions: A review

Antti I. Koponen

Address: VTT Technical Research Centre of Finland Ltd., P.O. Box 1603, FIN-40401 Jyväskylä, Finland

E-mail: Antti.Koponen@vtt.fi

Keywords: microfibrillated cellulose, nanofibrillated cellulose, cellulose microfibrils, cellulose nanofibrils, rheology, yield stress, viscosity, shear thinning, consistency

Abstract

While the raw material type and the production method of micro- and nanofibrillated celluloses (MNFC) strongly affect the absolute values of the rheological parameters of their aqueous suspensions, the dependence of these parameters on consistency, c, is found to be uniform. The consistency index and yield stress of MNFC suspensions follow generally the scaling laws $K : c^{2.43}$ and $t_y : c^{2.26}$, respectively, and a decent approximation for flow index is $n = 0.30 \times c^{-0.43}$. The variability of reported scaling exponents of these materials is likely mainly due to experimental uncertainties and not so much due to fundamentally different rheology. It is suggested that the reason behind the apparently universal rheological behavior of MNFC suspensions is the strong entanglement of fibrils; the flow dynamics of typical MNFC suspensions is dominated by interactions between fibril flocs and not by interactions between individual fibrils.

Introduction

Micro/nanofibrillated cellulose (MNFC), or cellulose micro/nanofibrils, has been a topic of academic interest since the 1980's due to its unique properties, such as mechanical robustness (it is stable over the whole pH range, at high salt concentrations, and at high temperatures), barrier properties, high specific surface area, lightness, and complex rheology. More recently, MNFC has also been perceived as a versatile, sustainable, and biodegradable material that enables developing eco-friendly all-cellulose products. The industrial interest in MNFC has recently increased also due to the rising number of commercially available MNFC grades. (Klemm et al. 2011)

MNFC fibrils can be isolated from wood or plant cell walls with a purely mechanical treatment, or with a chemical or enzymatic pretreatment followed by a mechanical treatment (Nechyporchuk et al.

1

2016)(Desmaisons et al. 2017). The fibrils may greatly differ in size and morphology depending on the fibrillation method used (see Figure 1.) Typically, the lateral dimension of fibrils is on the nanometer scale, and the length is up to several micrometers. The aspect ratio and the number of fibril-fibril contacts can, thus, be very high. The specific surface area (and, thus, hydroxyl group surface density) is also much higher than for regular cellulose fibers. For these reasons, MNFC suspensions can form yield-stress gels already at approx. 0.1 - 0.3% consistency (Varanasi et al. 2013) (Raj et al. 2016) (Li et al. 2016) (Arola et al. 2018), and they have a strong tendency towards aggregation and flocculation (Karppinen et al. 2012) (Pääkkönen et al. 2016) (Hubbe et al. 2017)(Raj et al. 2017) (Koponen et al. 2018).
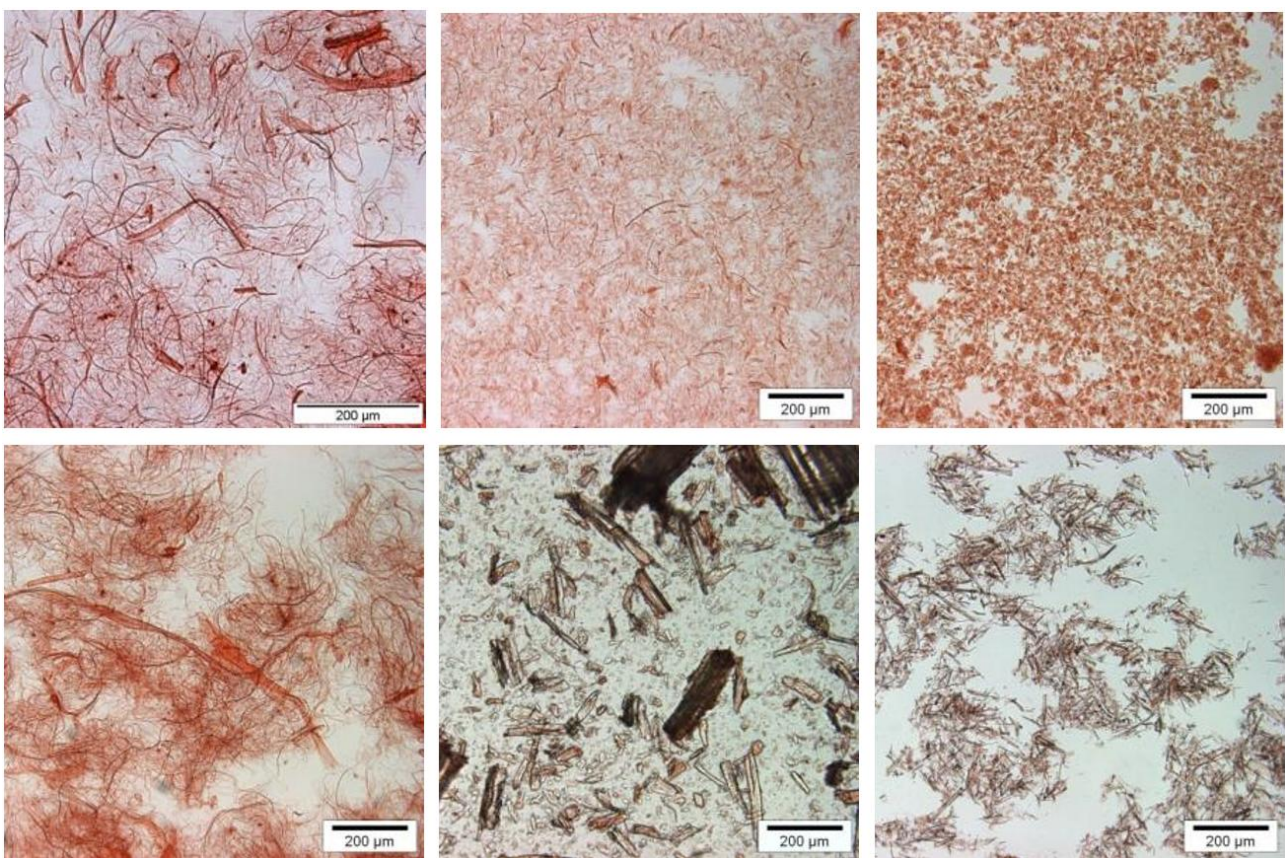

Figure 1. Examples of various types of MNFC fibrils.

The rheological characteristics of various MNFC suspensions has become a widely discussed topic. Although knowledge on rheological behavior is naturally important in the use of MNFC as a rheology modifier (Dimic-Misic et al. 2013)(Shao et al. 2015)(Li et al. 2015) and stabilizer (Andresen & Stenius 2007)(Winuprasith & Suphantharika 2013), such information is also needed for MNFC production (Delisée et al. 2010)(Pääkkönen et al. 2016)(Colson et al. 2016) and for other MNFC-related processes (Saarikoski et al. 2015) (Shao et al. 2015)(Hoeng et al. 2017) (Kumar et al. 2017). A recent thorough review of the rheology of MNFC suspensions can be found in (Hubbe et al. 2017).

As MNFC suspensions are non-Newtonian yield stress materials, the viscous (shear-thinning) behavior of aqueous MFCN suspensions is sometimes analyzed in the context of the Herschel-Bulkley equation (Mohtaschemi et al. 2014)

$$t = t_y + K \dot{\gamma}^n .$$ (1)

Above, t is the shear stress, t_y is the yield stress, $\dot{\gamma}$ is the shear rate, K is the consistency index, and n is the flow index. The use of Eq. (1), however, necessitates very accurate measurements, especially with small shear rates where, e.g., the effect of slip flow on the geometry boundaries (Buscall, 2010)(Saarinen et al. 2014) has been successfully eliminated. In practice, the rheological behavior of MFCN suspensions is usually described by the power law

$$m = K \dot{\gamma}^{n-1}$$ (2)

(Lasseuguette et al. 2008)(Moberg et al. 2014)(Mohtaschemi et al. 2014)(Honorato et al. 2015). Note that it has been suggested that the consistency index K reflects individual fibril characteristics, whereas the flow index n reflects the structural property of the whole suspension (Tatsumi et al. 2002).

For suspensions with elongated particles shear thinning becomes more pronounced as the particle aspect ratio, particle flexibility, or consistency increases (Goto et al. 1986)(Switzer & Klingenberg 2003)(Bounoua et al. 2016). An explanation of shear thinning, which works well for polymers (Wagner et al. 2014), is the alignment of particles due to shear. Owing to the high entanglement of fibrils, this is unlikely a sufficient mechanism for most MNFC suspensions. The mechanism behind the shear-thinning behavior of MNFC suspensions, which is also seen with other fibrous materials (Mongruel & Cloitre 1999)(Switzer & Klingenberg 2003)(Derakhshandeh et al. 2011)(Jiang et al. 2016), is likely to be caused by (adhesive) interactions between the fibrils. Hydrodynamic shear forces are more effective in breaking fibril-fibril contacts when the shear rate increases; this is reflected in a decrease in floc size and an increase in the orientation of the fibrils. As a result, the efficiency of momentum transport in the suspension declines and the viscosity decreases (Petrich et al. 2000)(Iotti et al. 2011)(Bounoua et al. 2016). This view is supported by the observation that in pulp suspensions, with a given shear rate, decreasing floc size decreases the viscosity of the suspension (Kerekes, 2006).
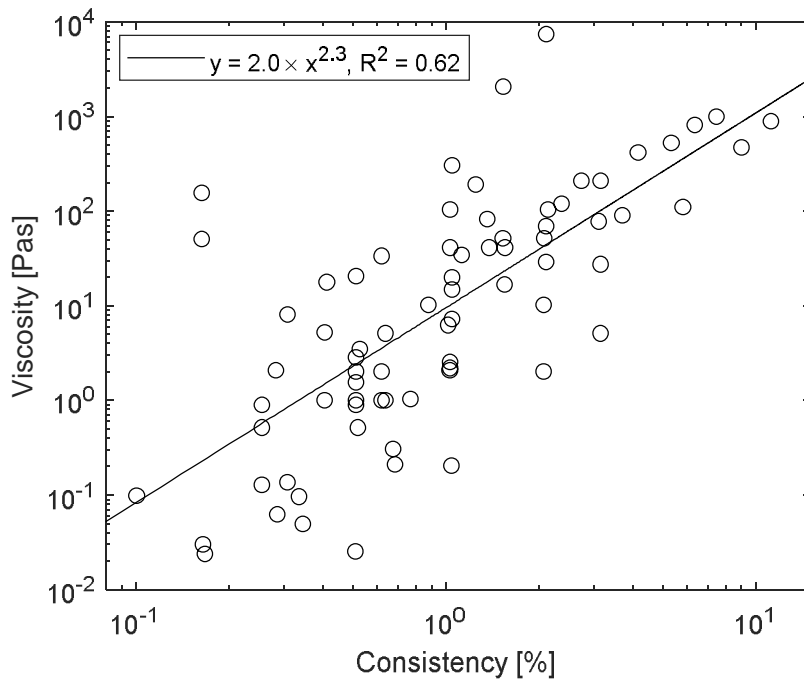
Figure 2. Viscosity of various aqueous MNFC suspensions as a function of consistency at the shear rate of 1.0 1/s. The data was collected from 40 studies (Hubbe et al. 2017). The aqueous solutions had water-like viscosity (not dominated by polyelectrolytes) and a wide range of ionic strengths, surface charges, and other details of experimentation. The solid line is a power law fit to the data. (To avoid the disturbing effect of outliers, which are common in the datasets analyzed here, we used the Matlab `robustfit` function throughout this study for fitting. The MATLAB version was 9.5.0.944444, R2018b).

Factors that affect the rheological properties of standard MNFC suspensions and, thus, also the values of parameters K and n in Eqs. (1) and (2), fall into several categories. One is morphology, which includes fibril flexibility and shape, length and diameter distributions, aspect ratio, fibrillation, and network/floc structure. Another factor is the surface-chemical composition of the fibrils, which can affect surface charge and the colloidal interactions between them. Both morphology and surface composition can depend on the processes of treatments used to prepare the material. The most universal parameter that affects MNFC rheology is indisputably mass consistency. Dimensional analysis shows that for flows of spherical non-Brownian surface-chemically neutral particles, the viscosity of a suspension is a function of only two factors: consistency and the viscosity of the carrier fluid; particle size does not affect it (Mewis & Wagner, 2012). Aspect ratio is another key parameter for elongated particles in this context. Two suspensions can, thus, have very similar viscous behavior even though their particle size differs considerably. Note that the tendencies of cellulosic materials to swell in water may differ, depending on their morphology and surface chemistry (Hubbe et al. 2017).

Consequently, the solids volume fractions of MNFCs may be different even though their mass consistencies are identical.

While the values of parameters K and n have been reported for MNFC suspensions in numerous studies, there are only a few studies where the dependence of the consistency index K and the flow index n on consistency have been studied systematically. In (Schenker et al. 2018) and (Turpeinen et al. 2019) these relations were found to be power laws, i.e. $K : c^{m_K}$ and $n : c^{m_n}$, where c is the mass consistency of the suspension. Note that similar scaling behavior is well known for the storage modulus G' and the loss modulus G'' of MNFC suspensions (Tatsumi et al. 2002)(Pääkkö et al. 2007)(Naderi & Lindström 2014)(Quennouz et al.2016). A power law relation, $t_y : c^{m_t}$ has been reported for yield stress in several studies (Lowys et al.2001)(Tatsumi et al. 2002) (Varanasi et al. 2013) (Mohtaschemi et al. 2014)(Kumar et al. 2016).

Figure 2 shows the viscosity of various MNFC suspensions as a function of consistency with a fixed shear rate (Hubbe et al. 2017). The figure shows that there is great variability in the viscosity values caused, e.g., by different raw materials and production methods, which result in great versatility in fibril shape, flexibility, fibrillation, entanglements, and surface chemistry. (Hubbe et al. 2017) conclude that, due to this divergent nature of MNFC materials, "the relationship between measured viscosity and nanocellulose solids content is likely to be irregular," and not necessarily conform to any of the many viscosity formulae they reviewed. (Hubbe et al. 2017) also emphasizes the variability of exponent m_K in the scaling law $K : c^{m_K}$ in the literature. We believe that this view reflects well the current general opinion of the rheology of MNFC suspensions. However, while it is likely that no general formula can be found for predicting the viscosity of a given MNFC suspension a priori, it might still be possible to find useful general guidelines on its viscous behavior. Even in Figure 2, which includes an extensive collection of different MNFC materials in various conditions, the general trend appears to be a power law with $m : c^{2.3}$.

In this review, we examined the dependence of shear viscosity and the yield stress of aqueous MNFC suspensions on consistency. Our focus was on the three scaling laws of $K : c^{m_K}$, $n : c^{m_n}$ and $t_y : c^{m_t}$. We included such studies where the rheology of at least three different MNFC consistencies were analyzed. Moreover, we included only studies where the measurements were performed on original MNFC materials. Studies where, e.g., ionic strength was modified or polymers were added, have been excluded. The observed similarities in the shear rheology of various MNFC suspensions suggest that the shear rheology of MNFC suspensions is more universal than has previously been realized.

Materials

Table 1 lists the included studies together with the MNFC raw material, MNFC manufacturing method, and the fibril dimensions. The aspect ratio was calculated from the middle values of the given length and width ranges. The fibril dimension of (Moberg et al. 2014) in Table 1 was obtained from (Wågberg et al., 2008), and the dimensions of unfiltered Celish fibrils of (Kataja et al. 2017) and (Turpeinen et al. 2019) in the table are from (Tatsumi et al. 2002). (Varanasi et al. 2013) used the finest 20% fraction of Celish, which explains their much smaller fibril dimensions when compared to those given by (Tatsumi et al. 2002). The length of fibrils made from softwood by using mechanical treatment in (Schenker et al. 2018), (Schenker et al. 2019), and (Turpeinen et al. 2019) is a rough estimate based on the fact that the width of the wall depletion layer of this MFC is one tenth of the wall depletion layer of native Celish (Turpeinen et al. 2019). The rheological analysis of the measurement data presented in (Kataja et al. 2017) can be found in (Koponen et al. 2019).

Table 1. From left to right: reference, raw material, manufacturing method (purely mechanical/purely chemical/pretreatment before mechanical disintegration), is sonication used as post treatment for dispergation, MNFC classification by (Hubbe et al. 2017), fibril length, fibril width, and fibril aspect ratio.

Reference	Raw material	Treatment	Son.	Type	Length [µm]	Width [nm]	AR
Lowys et al. 2001	sugar beet	purely chemical	-	MFC	-	-	-
Tatsumi et. al. 2002	cotton, CF11	purely chemical	x	NFC	0.7	17	24
Pääkkö et al. 2007	softwood	entzymatic	-	NFC	-	10	-
Lasseuguette et al. 2008	pinus pinaster	TEMPO-oxidized	x	NFC	-	-	50
Agoda-Tandjawa et al. 2010	sugar beet	purely chemical	x	MFC	< 10	2 - 15	-
Charani et al. 2013	kenaf bast	entzymatic	-	MFC	1 <	< 100	-
Varanasi et al. 2013	Celish	mechanical	-	MFC	8	50	140
Moberg et al. 2014	softwood	carboxymethylation	x	MFC	< 1	5 - 15	-
Mohtaschemi et al. 2014	birch	TEMPO-oxidized	-	NFC	1 - 10	2 - 6	1300
Honorato et al. 2015	pine, euca	TEMPO-oxidized	-	NFC	-	5 - 10	.
Kumar et al. 2016	softwood	mechanical	-	MFC	-	20 - 500	-
Nazari et al. 2016	softwood	mechanical	-	MFC	-	10 - 500	-
Quennouz et al. 2016	wood	TEMPO-oxidized	-	NFC	0.5	5	100
Geng et al. 2017	jute	TEMPO-oxidized	x	NFC	-	5	-
Kataja et al. 2017	Celish	mechanical	-	MFC	350	15×10^3	23
Schenker et al. 2018	eucalyptus	mechanical	x	MFC	~ 35	-	-
Schenker et al. 2019	eucalyptus	mechanical	x	MFC	~ 35	-	-
Turpeinen et al. 2019	Celish	mechanical	-	MFC	350	15×10^3	23
	birch	mechanical	-	MFC	~ 35	-	-

Table 1 shows that there is great variability in the fibril dimensions and aspect ratios among the different studies. This likely reflects both the great versatility of MNFC materials as well as

experimental uncertainties related to the measurement of width and length distributions. Due to their small size and often very wide width and length distributions, measuring the average diameter, not to mention the average length, is very challenging for MNFC materials. For this reason, the fibril dimensions shown in Table 1 may not be commensurate.

Table 2 shows the consistency range, the number of measured consistencies, the shear rate region, the existence of yield stress analysis, and the rheometer geometry used. In some cases, the lowest consistencies are close to or even below the gel point of the MNFC suspension, see e.g. (Geng et al. 2017) and (Lasseuguette et al. 2008). Some studies have reported the flow index K and the power index n explicitly for every consistency. However, in many studies, this data was not given. When that occurred, a graphical interface (`grabit` function written by Jiro Doke for Matlab) for acquiring viscosity-shear rate data from the figures was used, and the power law in Eq. (2) was fitted to the data. As discussed in next paragraph, shear rate regions with suspicious behavior were sometimes excluded from this analysis. In such cases the original values of K and n reported by the authors were not used.

Table 2. From left to right: reference, consistency range, number of consistencies, shear rate region, is the yield stress analyzed, and the rheometer geometry used (cp - cone and plate, pp - plate plate, bc - bob and cup, r - roughened or serrated walls).

Reference	c [%]	#	$\dot{\gamma}$ [1/s]	τ_y	Rheometer
Lowys et al. 2001	0.1 - 1.0	9	0.01	x	cp
Tatsumi et. al. 2002	0.1 - 3.0	4	0.01 - 60	x	pp
Pääkkö et al. 2007	0.1 - 6.0	7	0.1 - 1000	-	pp, cp
Lasseuguette et al. 2008	0.05 - 0.8	6	0.01 - 100	-	cp
Agoda-Tandjawa et al. 2010	0.3 - 3.0	7	0.01 - 100	-	pp
Charani et al. 2013	0.5 - 2.3	4	0.01 - 100	-	pp-r
Varanasi et al. 2013	0.2 - 1.5	5	-	x	vane
Moberg et al. 2014	0.5 - 1.0	3	0.1 - 500	-	cp
Mohtaschemi et al. 2014	0.3 - 1.0	4	0.01 - 100	x	vane
Honorato et al. 2015	0.1 - 1.0	3	2 - 1000	-	pp
Kumar et al. 2016	1.0 - 3.0	3	$250 - 10^4$	x	slot
Nazari et al. 2016	2.0 - 7.0	5	0.1 - 10	x	pp
Quennouz et al. 2016	0.3 - 1.2	3	0.01 - 100	x	cp-r
Geng et al. 2017	0.01 - 0.6	4	0.1 - 100	-	bc-r
Kataja et al. 2017	0.4 - 1.6	3	2 - 300	x	pipe
Schenker et al. 2018	0.5 - 2.0	3	0.01 - 1000	x	vane-r
Schenker et al. 2019	0.5 - 2.0	4	0.01 - 1000	x	vane-r
Turpeinen et al. 2019	0.2 - 1.5	6	1 - 200	x	pipe
	0.5 - 2.0	3	1 - 1000	x	pipe

In e.g. (Agoda-Tandjawa et al. 2010), the shear rate-viscosity rheograms have two shear rate regions with different slope and a plateauing region between them. In contrast, in e.g. (Tatsumi et al. 2002), the shear stress-shear rate rheograms have regions where shear stress is constant. In both studies the shear stress was probably below the yield stress, and slip flow had probably taken place at the lowest shear rates (Vadodaria et al. 2018)(Turpeinen et al. 2019). With higher shear rates; see e.g. (Charani et al. 2013); power law behavior was, in some cases, violated - probably due to some measurement-related instabilities. We have, whenever possible, excluded these shear rate regions from our analysis, and the shear rate region used for fitting the power law in Eq. (2) to the measurement data are then smaller than those shown in Table 2. (Nazari et al. 2016) have performed their measurements with exceptionally high shear rates. It seems that viscosity had saturated at the highest shear rates in their measurements. We have eliminated these measurement points from the analysis. In (Mohtaschemi et al. 2014), Herschel-Bulkley Eq. (1) was used successfully in the rheological analysis. We have used these values for parameters K and n.
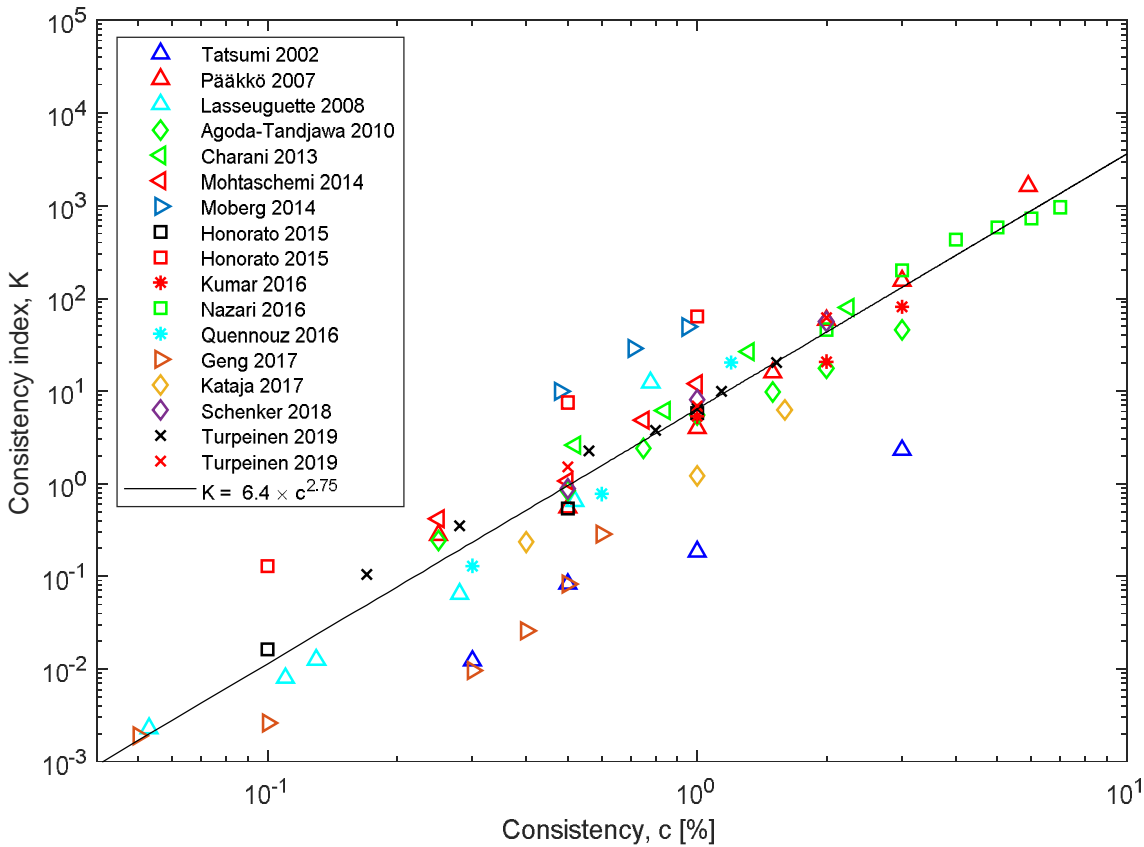

Figure 3. Consistency index K of Eq. (2) as a function of consistency obtained from different studies. The solid line is a power law fit to the data.

Finally note that, in a given consistency range, the values of the consistency index K can vary several orders of magnitude with different consistencies (see Figure 3), while the variation of the flow index

n is much smaller (see Figure 5.). For this reason, small discrepancies in the experimental setup (such as slip flow) do not have a big effect on the relative size of the values of *K* with different consistencies. The values of *n*, however, may, in such cases, be distorted much more, which is manifested, e.g., in the nonmonotous behavior of *n* as a function of consistency.

Table 3. Parameters K_0 and m_K of Eq. (3) and n_0 and m_n of Eq. (5) obtained with the fit to the data shown in Figure 3 and Figure 5. Note that, for (Lasseuguette et al. 2008) and (Geng et al. 2017), the obvious outliers (see Figure 4) at 0.8% and 0.05%, respectively, have been omitted from the fits.

Reference	*c* [%]	K_0	m_K	n_0	$-m_n$
Tatsumi et. al. 2002	0.1 - 3.0	0.22	2.15	0.31	0.078
Pääkkö et al. 2007	0.1 - 6.0	6.5	2.90	0.23	0.13
Lasseuguette et al. 2008	0.05 - 0.5	2.1	2.44	0.43	0.31
Agoda-Tandjawa et al. 2010	0.25 - 3.0	4.3	2.11	0.32	0.10
Charani et al. 2013	0.5 - 2.3	12	2.41	0.22	-0.44
Moberg et al. 2014	0.5 - 1.0	58	2.36	0.30	0.59
Mohtaschemi et al. 2014	0.25 - 1.0	9.5	2.43	0.28	0.40
Honorato et al. 2015	0.1 - 1.0	4.4	2.48	0.49	0.30
	0.1 - 1.0	57	2.67	0.37	0.30
Kumar et al. 2016	1.0 - 3.0	4.9	2.43	0.31	0.26
Nazari et al. 2016	2.0 - 7.0	13	2.31	0.17	0.24
Quennouz et al. 2016	0.3 - 1.2	8.1	3.64	0.21	1.0
Geng et al. 2017	0.1 - 0.6	0.40	2.39	0.47	0.32
Kataja 2017	0.4 - 1.6	1.7	2.30	0.35	0.30
Schenker et al. 2018	0.5 - 2.0	8.0	2.80	0.29	0.43
Turpeinen et al. 2019	0.2 - 1.5	7.1	2.37	0.27	0.37
	0.5 - 2.0	8.6	2.68	0.26	0.26
mean ± stdev			2.52 ± 0.37	0.31 ± 0.10	0.29 ± 0.29

Shear viscosity

Figure 3 shows the consistency index *K* as a function of consistency for different studies. The figure shows that the consistency index usually follows a power law

$$K = K_0 c^{m_K} , \tag{3}$$

where K_0 and m_K are MNFC-dependent material parameters. Table 3 shows the values of K_0 and m_K for different MNFCs. We can see that K_0 varies strongly; the difference between lowest and highest values being more than two orders of magnitude. The exponents m_K, in contrast, are quite close to each other.

A power law fit to all the data points in Figure 3 gives $K = 6.4 \times c^{2.75}$. However, the exponent is rather sensitive to the distribution of data points, and it does not necessarily accurately reflect the true average behavior of these materials. A better estimate is obtained by doing the analysis for the normalized consistency index $\bar{K} = K/K_0$ (see Figure 4). Then, the power law fit gives

$$\bar{K} = 0.98 \times c^{2.43}. \tag{4}$$

Figure 4 shows that while there are some outliers, all MNFCs generally follow very well the power law in Eq. (4). (Lowys et al. 2001), (Lasseuguette et al. 2008) and (Geng et al. 2017) have shown that the slope of the viscosity versus consistency curve is much shallower and the flow is almost Newtonian below the gel point. In Geng et al. e.g., the viscosity of the NFC suspension scaled as $m: c^{0.4}$ below the gel point of 0.2% (with shear rate 100 1/s). In Figure 4, the deviation of the two low consistency data points of (Geng et al. 2017) from the general trend is due to this behavior.
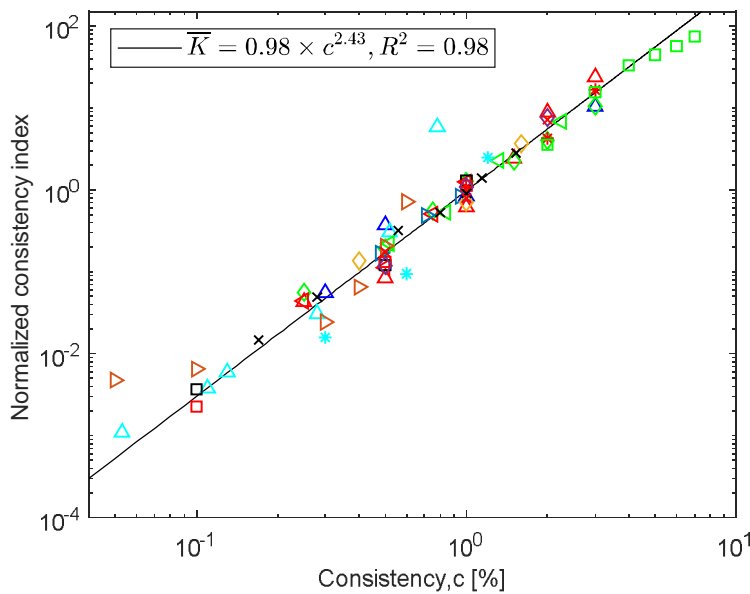

Figure 4. Normalized consistency index $\bar{K} = K/K_0$ as a function of consistency. The markers are the same as in Figure 3. A power law fit to the data gives $K : c^{2.43}$.

Figure 5 shows the flow index n as a function of consistency for different studies. We can see in the figure that there are several outliers, and in many cases, the values of n do not decrease monotonously with increasing consistency.

Table 3 shows the values of n_0 and m_n of a power-law fit

$$n = n_0 c^{m_n} \tag{5}$$

for different MNFCs. We can see that while n_0 is of the same order in all cases, the variation of m_n is rather high. It is likely that many of these variations are due to experimental uncertainties and not due to fundamental differences in the rheological behavior of these materials. This possibility is emphasized by the fact that the biggest deviations from the average were obtained with either smooth plate-plate or smooth cone-and-plate geometries (compare Table 2 and Table 3 3), which are rather sensitive geometries to slip flow. The solid line in Figure 5 is a power law fit of Eq. (5) to all data points:

$$n = 0.30 \times c^{-0.43}. \tag{6}$$

This equation gives a reasonable approximation of the general rheological behavior of the flow index n of MNFC suspensions.
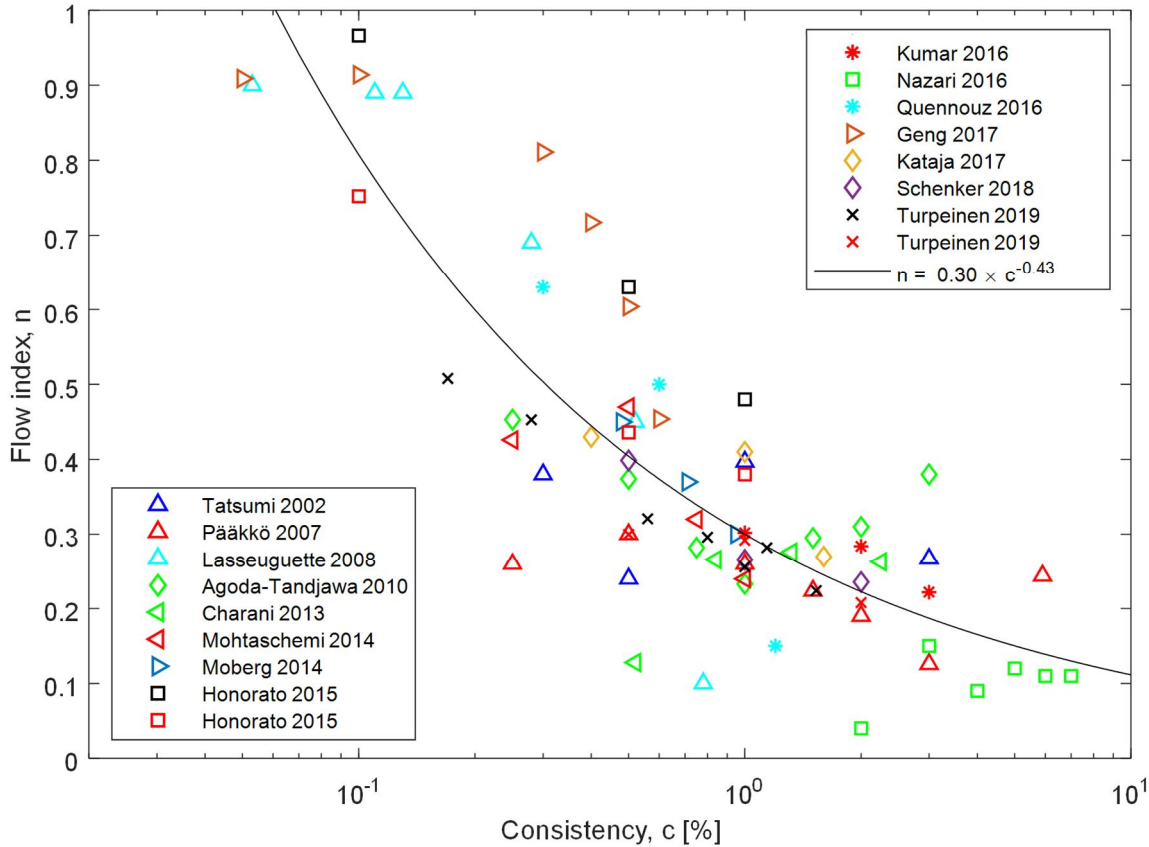

Figure 5. Flow index n of Eq. (2) as a function of consistency obtained from different studies. The solid line is a power law fit to the data.

By combining Eqs. (4) and (6), we get the following general formula for the viscosity of MNFC suspensions:

$$m(c, \dot{\gamma}) = M \times c^{2.43} \dot{\gamma}^{n-1}; \; n = 0.30 \times c^{-0.43}. \tag{7}$$

11

Above M is a material parameter that depends on the MNFC grade. Table 4 shows the values of M for various MNFCs. We can see in the table that, in most cases, M is close to K_0 - in an ideal case they would be equal.

Table 4. Parameter M for various MNFC materials. Also shown are M/K_0, and the mean and standard deviation of d defined in Eq. (8).

Reference	c [%]	M	M/K_0	mean(δ)	std(δ)
Tatsumi et. al. 2002	0.3 - 3.0	0.23	0.96	0.36	0.28
Pääkkö et al. 2007	1.0 - 6.0	6.1	0.66	0.45	0.26
Lasseuguette et al. 2008	0.05 - 0.5	2.6	0.80	0.50	0.44
Agoda-Tandjawa et al. 2010	0.3 - 3.0	4.5	0.96	0.24	0.25
Charani et al. 2013	0.5 - 2.3	11.3	1.03	0.24	0.16
Moberg et al. 2014	0.5 - 1.0	70	0.83	0.17	0.10
Mohtaschemi et al. 2014	0.3 - 1.0	10.0	0.95	0.24	0.28
Honorato et al. 2015	0.1 - 1.0, pine	5.8	0.76	0.62	0.59
	0.1 - 1.0, euca	46	1.25	0.32	0.19
Kumar et al. 2016	1.0 - 3.0	5.6	0.87	0.16	0.20
Nazari et al. 2016	3.0 - 7.0	8.0	1.62	0.33	0.41
Quennouz et al. 2016	0.3 - 1.2	5.7	1.44	0.70	0.68
Geng et al. 2017	0.1 - 0.6	0.38	1.05	0.75	0.68
Kataja 2017	0.4 - 1.6	2.1	0.82	0.21	0.34
Schenker et al. 2018	0.5 - 2.0	7.2	1.03	0.30	0.18
Turpeinen et al. 2019	0.2 - 1.5, Celish	6.9	1.03	0.16	0.18
	0.5 - 2.0, birch	7.7	1.12	0.26	0.18
mean			1.01	0.35	0.32

Figure 6 shows the viscosity given by Eq. (7) as a function of viscosity calculated from Eq. (2) for all the MNFCs shown in Table 4 for shear rates of 0.1, 1.0, 10, 100, and 1000 1/s. The correlation between these values is seen to be very high ($R^2 = 0.99$). Table 4 shows the mean and standard deviation for the various MNFCs of

$$d(\dot{\gamma},c) = \frac{\left| m(\dot{\gamma},c)_{\text{model}} - m(\dot{\gamma},c)_{\text{exp}} \right|}{m(\dot{\gamma},c)_{\text{exp}}}, \tag{8}$$

where $m(\dot{\gamma},c)_{\text{model}}$ and $m(\dot{\gamma},c)_{\text{exp}}$ are the modelled and measured viscosity for shear rate $\dot{\gamma}$ and consistency c, respectively. As we can see in Table 4, there is considerable variation in the values of mean(δ) and std(δ). For most MNFCs, Eq. (7) gives viscosity with a good accuracy, while for some MNFCs, the accuracy is only decent. This difference can also be seen in Figure 6, where blue and red circles show the best case (Moberg et al. 2014) and the worst case (Geng et al. 2017), respectively.
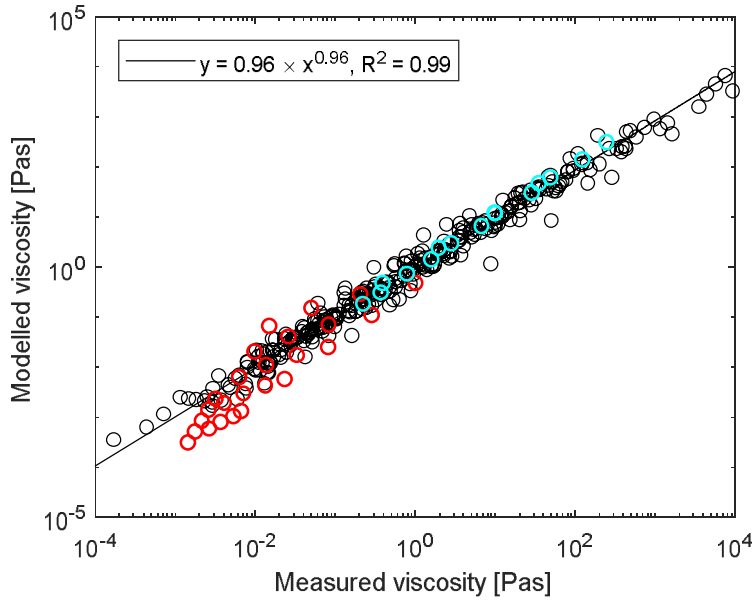
Figure 6. The viscosity given by Eq. (7) as a function of viscosity calculated from Eq. (2) for all the MNFCs shown in Table 4. The viscosities were calculated for shear rates of 0.1, 1.0, 10, 100, and 1000 1/s. The solid line shows a power law fit to the data. Blue and red circles show the best case (Moberg et al. 2014), $R^2 = 1.00$, and the worst case (Geng et al. 2017), $R^2 = 0.84$, respectively.
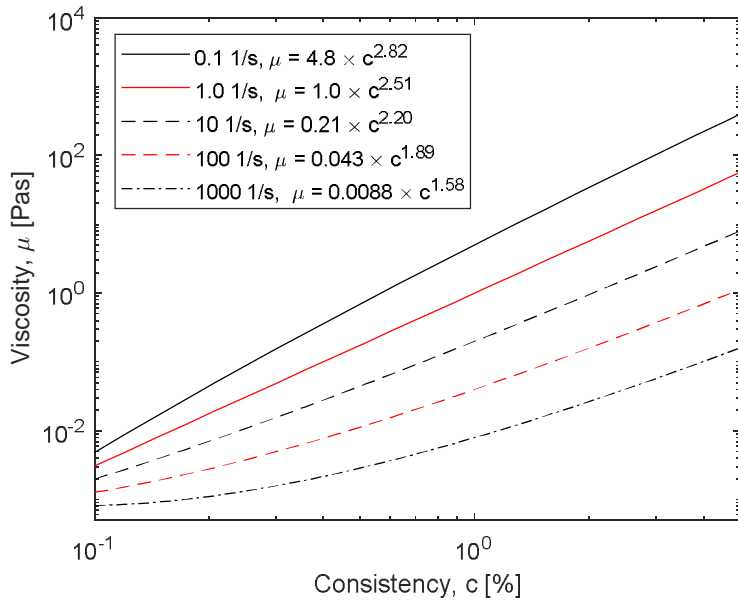

Figure 7. Viscosity given by Eq. (7) with $M = 1$ for various shear rates. The power law fit was performed for the consistency range of 0.3 - 3%.

In the literature, the consistency dependence of the viscosity of MNFC suspensions is often given in the simple form of m: c^m (Hubbe et al. 2017). This is, however, misleading, as parameter m is not unique but depends on the shear rate. Figure 7 shows as an example the viscosity given by Eq. (7) for various shear rates with $M = 1$. Also shown are power law fits for each shear rate. We can see in the

figure that exponent m increases from 1.6 to 2.8 when the shear rate decreases from 1000 1/s to 0.1 1/s.
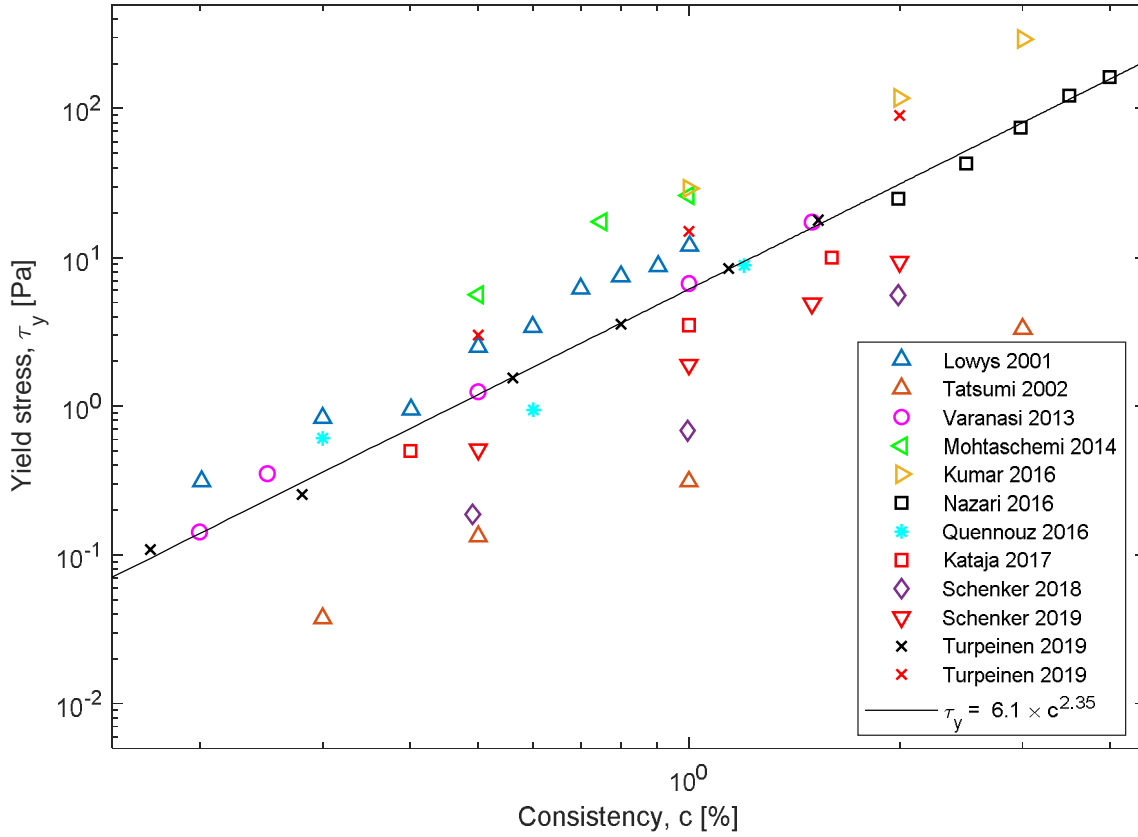

Figure 8 Yield stress as a function of consistency for different studies. The solid line shows a power law fit to the data.

Yield stress

Figure 8 shows the yield stress t_y as a function of consistency for different studies. We can see that, just like the consistency index, the yield stress also follows a power law

$$t_y = t_0 c^{m_t} , \qquad (9)$$

where τ_0 and m_τ are MNFC-dependent parameters. Table 5 shows the values of τ_0 and m_τ for different MNFCs. According to (Bennington et al. 1990) τ_0 depends on Young's modulus and the aspect ratio of the fibrils. We can see in the figure that τ_0 varies strongly; the difference between lowest and highest value is more than two orders of magnitude. The exponents m_τ, on the other hand, are quite close to each other. Notice that there was no correlation between parameters K_0 and τ_0. Thus, the absolute levels of viscosity and yield stress appear to be uncorrelated. (This is also reflected in the high variability of parameter a in Table 6.) It is possible that the experimental uncertainties discussed

14

below are too high and the dataset is too small for this analysis. However, this surprising finding merits further investigation.

Table 5. Parameters τ_0 and m_τ of Eq. (9) obtained with a power law fit to the data shown in Figure 8.

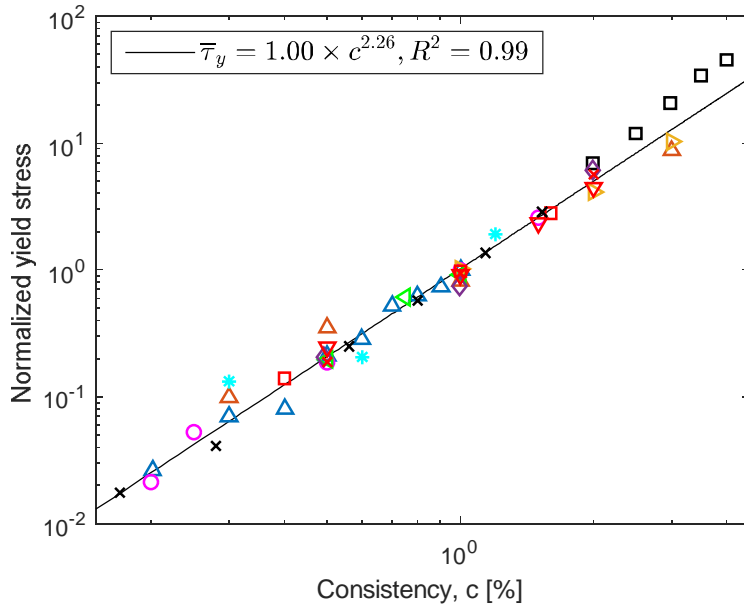| Reference	c [%]	τ_0	m_τ
Lowys et al. 2001	0.3 - 1.0	12	2.25
Tatsumi 2002	0.3 - 3.0	0.38	2.04
Varanasi et al. 2013	0.2 - 1.5	6.7	2.30
Mohtaschemi et al. 2014	0.5 - 1.0	28	2.25
Kumar et al. 2016	1.0 - 3.0	29	2.10
Nazari et al. 2016	2.0 - 4.0	3.6	2.77
Quennouz et al. 2016	0.3 - 1.2	4.6	1.93
Kataja 2017	0.4 - 1.6	3.6	2.16
Schenker et al. 2018	0.5 - 2.0	0.91	2.42
Schenker et al. 2019	0.5 - 2.0	2.1	2.10
Turpeinen et al. 2019	0.2 - 1.5	6.2	2.49
	0.5 - 2.0	16	2.45
mean ± stdev			2.27 ± 0.23

Figure 9. Normalized yield stress $\bar{\tau}_y = \tau_y/\tau_0$ as a function of consistency. The markers are the same as in Figure 8. A power law fit to the data gives $\tau_y : c^{2.26}$.

A power law fit to all the data points in Figure 8 gives $\tau_y = 6.1 \cdot c^{2.35}$. A corresponding fit to the normalized yield stress $\bar{\tau}_y = \tau_y/\tau_0$ gives (see Figure 9)

$$\bar{t}_y = 1.00 \times c^{2.26}.$$ (10)

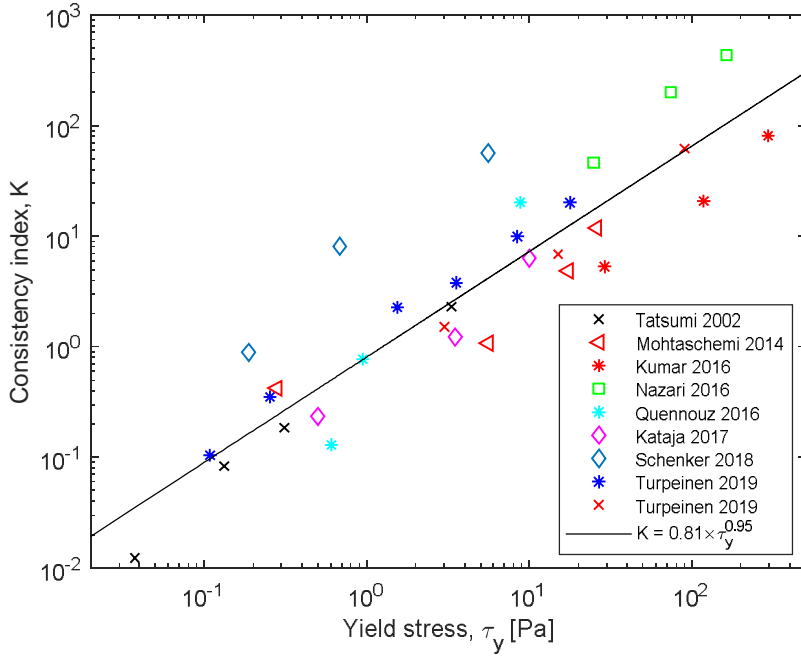We can see in Figure 9 that most MNFCs follow very well the power law in Eq. (10).

Figure 10. Consistency index K as a function of yield stress t_y. The solid line shows a power law fit to the data.

Relation between consistency index and yield stress

We can see from Eqs. (4) and (10) that the consistency dependence of K and t_y is almost identical. It is, thus, interesting to directly compare how these two quantities relate to each other. Figure 10 shows the consistency index as a function of the yield stress for studies where both quantities have been reported. Table 6 shows the values of parameters a and b for the power law

$$K = at_y^b.$$ (11)

We can see in Table 6 that, while there is great variation in a, the values of exponent b are, in most cases, quite close to each other. Figure 11 shows the normalized consistency index $\bar{K}_a = K/a$ as a function of yield stress. The solid line shows the power law fit

$$\bar{K}_a = 1.01 \times t^{1.12}$$ (12)

to the data. Most data points follow this formula very accurately. The relation between the consistency index and the yield stress is, consequently, generally almost linear.

16

Table 6. The fitting parameters of Eq. (11) for the data shown in Figure 10.

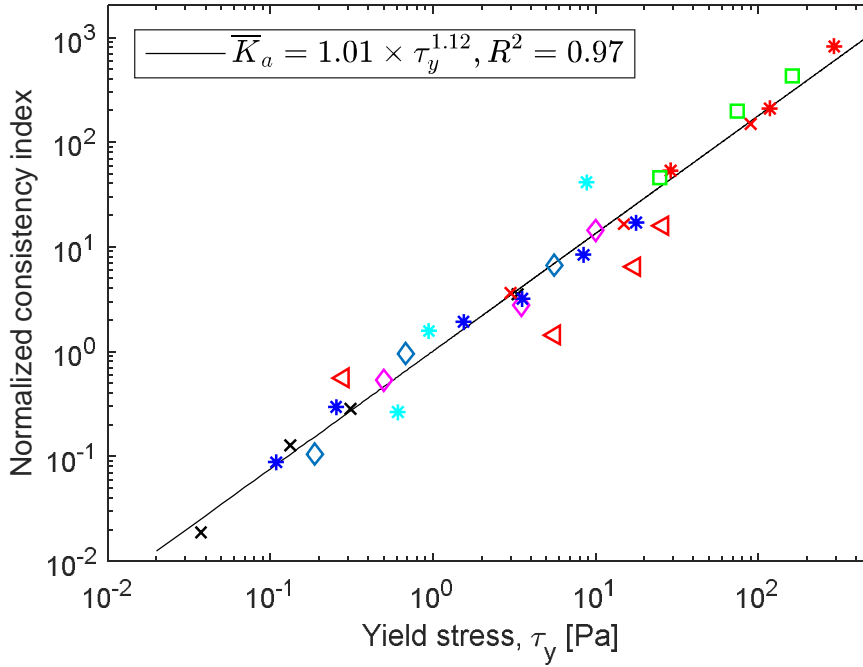| Reference	a	b
Tatsumi et. al. 2002	0.65	1.14
Mohtaschemi et al. 2014	0.75	0.67
Kumar et al. 2016	0.10	1.16
Nazari et al. 2016	1.0	1.20
Quennouz et al. 2016	0.49	1.75
Kataja 2017	0.44	1.07
Schenker et al. 2018	8.5	1.20
Turpeinen et al. 2019	1.2	1.00
	0.42	1.09
mean ± stdev		1.14 ± 0.28

Figure 11. Normalized consistency index $\overline{K}_a = K/a$ as a function of yield stress. The markers are the same as in Figure 10. The solid line shows a power law fit to the data.

Discussion

The rheological behavior of MNFC materials is often compared with pulp fiber suspensions. The yield stress of pulp suspensions also generally follows the power law in Eq. (9). In numerous studies, the values of m_τ have varied in the range of 1.6 - 3.3 (Bennington et al. 1990)(Huhtanen & Karvinen 2006) (Derakhshandeh et al. 2010a)(Derakhshandeh et al. 2011)(Sumida 2013). In (Dalpke & Kerekes 2005), e.g., exponent m_τ slowly approached the value of 2.4 (shorter fibers had a higher exponent) when the fiber length (or aspect ratio) increased, while in (Bennington & Kerekes 1996),

the energy dissipation needed for floc level fluidization of pulps scaled as $\sim c^{2.5}$. Due to experimental difficulties, relatively few studies have been devoted to measuring the viscosity of pulp suspensions. (Huhtanen & Karvinen 2006) used Eq. (3) and obtained $m_K = 1.8$, while in (Bennington & Kerekes 1996), the viscosity of pulp scaled as $\sim c^{3.1}$. In (Derakhshandeh et al. 2010b), however, the relation between consistency index and consistency was approximately linear. Experiments with pulp suspensions have, thus, with some exceptions, given scaling exponents similar to MNFC suspensions with an even wider variation, at least partly due to higher experimental uncertainties. However, there is enough similarity between the rheological behaviour of pulp and MNFC suspensions to speculate that similar mechanisms might take place during the shearing of them. Thus, in their basic form (i.e. with low ionic strength and without extra polymers or surface modification), MNFCs might rheologically be somewhat surprisingly simply another group of fibrous materials with a high aspect ratio, not too far from other fiber suspensions.

A possible reason for the observed similarity of the rheological behavior of most MNFCs (and possibly also for the similar behavior of pulp fiber suspensions) may be the strong entanglement of the MNFC fibrils. Micrographs of MNFC products usually show highly complex structures that are, similar to pulp suspensions (Kerekes et al. 1985), better described as networks of flocs rather than individual fibrils. Typical lengths of the aggregated MNFC structures are in the range of 20 to 1000 μm (Hubbe et al. 2017). Consequently, although the fibrils that compose MNFC can be clearly in the "nano" range, the gross structure is typically a lot larger. So, rather than having a suspension of individual fibrils, the rheology of a MNFC suspension might more appropriately be modelled as a suspension of flocs dispersed in a liquid phase or in a gel-like matrix (Saarikoski et al. 2012)(Hubbe et al. 2017). As a consequence, the behavior of different MNFC suspensions is similar at mesoscopic and macroscopic scales. Examples of dynamics of MNFC flocs can be found in (Saarikoski et al., 2012)(Saarinen et al., 2014)(Haavisto et al. 2015)(Koponen et al., 2018).

Eq. (3), with $m_K = 2.43$, and Eq. (9), with $m_\tau = 2.26$, are a useful starting point when analyzing the measured rheological data. If the obtained fitting values of K_{00} and τ_{00} differ significantly from the values K_0 and τ_0 (obtained with a fit that also has m_K and m_τ as fitting parameters), one should consider if the difference is real or due to experimental uncertainties. For the studies reviewed in the present study, K_{00} and τ_{00} were, in most cases, close to K_0 and τ_0. The two exceptions were (Nazari et al. 2016) where $K_{00}/K_0 = 0.84$ and $\tau_{00}/\tau_0 = 1.73$, and (Quennouz et al. 2016), where $K_{00}/K_0 = 0.51$ and $\tau_{00}/\tau_0 = 1.19$. As there is a clear difference only in either K_{00} or τ_{00}, it is likely that the discrepancy is due to experimental uncertainty and not due to exceptional rheology. Also, when comparing the general rheological behavior of different MNFCs, it might be useful to compare the values of K_{00} and τ_{00}

instead of K_0 and τ_0. If one wants to include shear thinning behavior into the analysis, Eq. (7), or its generalized version

$$m(c, \dot{\gamma}) = Wc^m \dot{\gamma}^{n-1}; \quad n = qc^{-p} \tag{13}$$

can be used. (*W, m, q* and *p* above are fitting parameters.) Due to high degrees of freedom, Eq. (13) usually fits very well (R^2 close to one) to the viscosity-shear rate data. Eq. (13) is, consequently, preferred if a good quantitative description of the data is required. However, the use of Eq. (7) should always be considered as it may give a better description of the real rheological behavior, especially outside the measurement range. Moreover, the singe-free fitting parameter *M* can then be used for comparing the general rheological behavior of different MNFCs.

Table 7. Fitting parameters of Eqs. (3), (5), and (9) for different rheometer geometries for a mechanically disintegrated MFC in the consistency range of 0.5 - 2.0% (bc - bob and cup, r - roughened or serrated walls, the gap size is in millimeters). The obtained power law parameters were found to grow/decrease rather systematically with improved rheometer geometry. Red and blue arrows show the direction of the increasing and decreasing tendency, respectively. (Schenker et al. 2018)

Rheometer	K_0	m_K	n_0	$-m_n$	τ_0	m_τ
bc, 1.7	1.1	3.1	0.39	0.0	-	-
bc, 2.7	1.3	2.9	0.41	0.27	0.20	2.69
bc-r, 2.7	2.0	2.8	0.37	0.30	0.18	2.71
vane-r, 6.9	8.0	2.8	0.29	0.43	0.91	2.42

Due to slip flow and flocculation, the shear viscosity of MNFC suspensions is exceptionally difficult to measure quantitatively with good accuracy (Saarinen et al. 2014). Slip flow may have influenced viscosity data considerably also when it is not apparent in the rheogram (Turpeinen et al. 2019). (Schenker et al. 2018) have studied shear viscosity and yield stress with different rheometer geometries. The difference between the measured viscosity and yield stress was found to be, in the worst cases, an order of magnitude. According to (Vadodaria et al. 2018), scientific literature on the rheological properties of MNFC is due to slip replete with such erroneous viscosity data. Note that for yield stress, a unique definition does not even exist, and different measurement techniques may give different results even though the measurements have been performed rigorously. (Nazari et al. 2016) have studied the yield stress of an MFC suspension with various methods on rotational rheometers (in the present article, we used their values obtained with a vane geometry) and found that the obtained yield stress values could vary as much as a factor of 4. Table 7 shows the fitting

parameters of Eqs. (3), (5), and (9) for different rheometer geometries for the viscosity and yield stress data of (Schenker et al. 2018). We can see in the table that, although the parameters K_0 and τ_0 vary significantly between the different rheometer geometries, parameters m_K and m_τ are rather close to each other. The variation of parameters n_0 and m_n is also rather small. While the reason behind this behavior warrants further study, it explains why the scaling behavior of shear viscosity and yield stress on consistency is often rather similar among different studies even though the measurement data may have in some cases been quantitatively wrong (i.e. erroneous K_0 or τ_0) due to slip flow.

Rough or serrated walls are often used to eliminate the slip at walls, but they may not solve the problem entirely for basic rotational geometries (see Table 7 and (Nechyporchuk et al. 2014)). However, vane-in-cup geometry, especially with a wide gap, has been found to decrease slip effects for both wood fiber suspensions (Mosse et al. 2012) and MNFC suspensions (Mohtaschemi et al. 2014). A wide gap, however, is not always problem-free. It may introduce heterogeneous flow in the vane geometry, which must be properly addressed in order to obtain correct results. A wide gap may also cause the system to be susceptible to secondary flows (Mohtaschemi et al. 2014). Finally notice that the effect of slip flow on the rheological analysis can be totally eliminated by combining the rheometer with a velocity profiling technique, such as Ultrasound Velocity Profiling (UVP), Nuclear Magnetic Resonance Imaging (MRI), or Optical Coherence Tomography (OCT) (Sanna Haavisto et al. 2017)(A. Koponen & Haavisto 2018). Of the studies reviewed here, this approach was used in (Kataja et al. 2017) and (Turpeinen et al. 2019).

Conclusions

Although it is obvious that MNFC raw material and production method strongly affect the absolute values of yield stress and the viscosity of MNFC suspensions, it seems that the scaling laws on consistency are similar for a wider group of MNFC materials than previously believed. The consistency index and yield stress of MNFC suspensions reviewed in this study generally followed the scaling laws $K : c^{2.43}$ and $t_y : c^{2.26}$, and the relation between the consistency index and the yield stress was almost linear. While the measured values of the flow index n varied - possibly mostly due to experimental uncertainties, a decent approximation for n was given by the formula $n = 0.30 \,´\, c^{-0.43}$.

The variability of the scaling law parameters of MNFC suspensions found in the literature (see Table 3 and Table 5) is probably not so much due to real differences in the physical behavior of the suspensions rather than due to experimental uncertainties and to general difficulties in measuring the rheological behavior of these suspensions rigorously. The reason behind the universal rheological

behavior at mesoscopic and macroscopic scales might be the strong entanglement of fibrils; the flow dynamics of typical MNFC suspensions is dominated by interactions between fibril flocs and not so much by interactions between individual fibrils.

The obtained scaling laws were used to form a general formula, Eq. (7), for MNFC viscosity as a function of shear rate and consistency. Although this formula has only one fitting parameter, it worked quite well for most MNFCs reviewed in this study. This formula can be a useful framework when interpreting and analyzing measured MNFC rheological data.

In the future, a corresponding analysis should be performed in the LVE-region for parameters of oscillatory rheology, i.e. for the storage modulus G' and the loss modulus G'', and their relation to the consistency index K and the yield stress τ_y.

Acknowledgements

Declaration of conflict of interest: The author declares no conflict of interest.

References

Agoda-Tandjawa, G., Durand, S., Berot, S., Blassel, C., Gaillard, C., Garnier, C., & Doublier, J. (2010). Rheological characterization of microfibrillated cellulose suspensions after freezing. *Carbohydrate Polymers*, *80*(3), 677–686. https://doi.org/10.1016/j.carbpol.2009.11.045

Andresen, M., & Stenius, P. (2007). Water-in-oil emulsions stabilized by hydrophobized microfibrillated cellulose. *Journal of Dispersion Science and Technology*, *28*(6), 837–844. https://doi.org/10.1080/01932690701341827

Arola, S., Ansari, M., Oksanen, A., Retulainen, E., Hatzikiriakos, S., & Brumer, H. (2018). The sol-gel transition of ultra-low solid content TEMPO-cellulose nanofibril/mixed-linkage β-glucan bionanocomposite gels. *Soft Matter*, *14*(46), 9393–9401. https://doi.org/10.1039/c8sm01878b

Bennington, C., & Kerekes, R. (1996). Power requirements for pulp suspension fluidization. *Tappi Journal*, *79*(2), 253–258.

Bennington, C., Kerekes, R., & Grace, J. (1990). The yield stress of fiber suspensions. *The Canadian Journal of Chemical Engineering*, *68*, 748–757.

Bounoua, S., Lemaire, E., Férec, J., Ausias, G., & Kuzhir, P. (2016). Shear-thinning in concentrated rigid fiber suspensions: Aggregation induced by adhesive interactions. *Journal of Rheology*, *60*(6), 1279–1300. https://doi.org/10.1122/1.4965431

Buscall, R. (2010). Letter to the Editor : Wall slip in dispersion rheometry. *Journal of Rheology, 54*, 1177–1183. https://doi.org/10.1122/1.3495981

Charani, R., Dehghani-Firouzabadi, M., Afra, E., & Shakeri, A. (2013). Rheological characterization of high concentrated MFC gel from kenaf unbleached pulp. *Cellulose*, *20*(2), 727–740. https://doi.org/10.1007/s10570-013-9862-1

Colson, J., Bauer, W., Mayr, M., Fischer, W., & Gindl-Altmutter, W. (2016). Morphology and rheology of cellulose nanofibrils derived from mixtures of pulp fibres and papermaking fines. *Cellulose*, *23*(4), 2439–2448. https://doi.org/10.1007/s10570-016-0987-x

Dalpke, B., & Kerekes, R. (2005). The influence of pulp properties on the apparent yield stress of flocculated fibre suspensions. *Journal of Pulp and Paper Science*, *31*(1), 39–43.

Delisée, C., Lux, J., & Malvestio, J. (2010). 3D morphology and permeability of highly porous cellulosic fibrous material. *Transport in Porous Media*, *83*, 623–636. https://doi.org/10.1007/s11242-009-9464-4

Derakhshandeh, B., Kerekes, R., Hatzikiriakos, S., & Bennington, C. (2011). Rheology of pulp fibre suspensions: A critical review. *Chemical Engineering Science, 66*(15). 3460-3470. https://doi.org/10.1016/j.ces.2011.04.017

Derakhshandeh, B., Hatzikiriakos, S., & Bennington, C. (2010a). The apparent yield stress of pulp fiber suspensions. *Journal of Rheology*, *54*(5), 1137–1154. https://doi.org/10.1122/1.3473923

Derakhshandeh, B., Hatzikiriakos, S., & Bennington, C. (2010b). Rheology of pulp suspensions using ultrasonic Doppler velocimetry. Rheologica Acta, 49(11), 1127–1140. https://doi.org/10.1007/s00397-010-0485-2

Desmaisons, J., Boutonnet, E., Rueff, M., Dufresne, A., & Bras, J. (2017). A new quality index for benchmarking of different cellulose nanofibrils. *Carbohydrate Polymers*, *174*, 318–329. https://doi.org/10.1016/j.carbpol.2017.06.032

Dimic-Misic, K., Gane, P., & Paltakari, J. (2013). Micro and nanofibrillated cellulose as a rheology modifier additive in CMC-containing pigment-coating formulations. *Industrial and Engineering Chemistry Research*, *52*(45), 16066–16083. https://doi.org/10.1021/ie4028878

Geng, L., Naderi, A., Zhan, C., Sharma, P., Peng, X., & Hsiao, B. (2017). Rheological properties of jutebBased cellulose nanofibers under different ionic conditions. In *Nanocelluloses: Their Preparation, Properties, and Applications* (pp 113–132). American chemical society.

Goto, S., Nagazono, H., & Kato, H. (1986). 'The flow behavior of fiber suspensions in Newtonian fluids and polymer solutions. I. Mechanical properties. *Rheologica Acta*, *25*(3), 246–256.

Haavisto, S., Salmela, J., Jäsberg, A., Saarinen, T., Karppinen, A., & Koponen, A. (2015). Rheological characterization of microfibrillated cellulose suspension using optical coherence tomography. *Tappi Journal*, *14*(5), 291–302.

Haavisto, Sanna, Cardona, M., Salmela, J., Powell, R., McCarthy, M., Kataja, M., & Koponen, A. (2017). Experimental investigation of the flow dynamics and rheology of complex fluids in pipe flow by hybrid multi-scale velocimetry. *Experiments in Fluids*, *58*(11), 1–13. https://doi.org/10.1007/s00348-017-2440-9

Hoeng, F., Denneulin, A., Reverdy-Bruas, N., Krosnicki, G., & Bras, J. (2017). Rheology of cellulose nanofibrils/silver nanowires suspension for the production of transparent and conductive electrodes by screen printing. *Applied Surface Science*, *394*, 160–168. https://doi.org/10.1016/j.apsusc.2016.10.073

Honorato, C., Kumar, V., Liu, J., Koivula, H., Xu, C., & Toivakka, M. (2015). Transparent nanocellulose-pigment composite films. *Journal of Materials Science*, *50*(22), 7343–7352. https://doi.org/10.1007/s10853-015-9291-7

Hubbe, M., Tayeb, P., Joyce, M., Tyagi, P., Kehoe, M., Dimic-Misic, K., & Pal, L. (2017). Rheology of nanocellulose-rich aqueous suspensions: a review. *Bioresources*, *12*(4), 9556–9661.

Huhtanen, J., & Karvinen, R. (2006). Characterization of non-Newtonian fluid models for wood fiber suspensions in laminar and turbulent flows. *Annual Transactions of the Nordic Society of Rheology*, *14*.

Iotti, M., Gregersen, O., Moe, S., & Lenes, M. (2011). Rheological studies of microfibrillar

cellulose water dispersions. *Journal of Polymers and the Environment*, *19*(1), 137–145. https://doi.org/10.1007/s10924-010-0248-2

Jiang, G., Turner, T., & Pickering, S. (2016). The shear viscosity of carbon fibre suspension and its application for fibre length measurement. *Rheologica Acta*, *55*(1), 1–10. https://doi.org/10.1007/s00397-015-0890-7

Karppinen, A., Saarinen, T., Salmela, J., Laukkanen, A., Nuopponen, M., & Seppälä, J. (2012). Flocculation of microfibrillated cellulose in shear flow. *Cellulose*, *19*(6), 1807–1819. https://doi.org/10.1007/s10570-012-9766-5

Kataja, M., Haavisto, S., Salmela, J., Lehto, R., & Koponen, A. (2017). Characterization of micro-fibrillated cellulose fiber suspension flow using multi scale velocity profile measurements. *Nordic Pulp & Paper Research Journal*, *32*(3), 473-482. https://doi.org/10.3183/NPPRJ-2017-32-03-p473-482

Kerekes, R., Soszynski, R., & Tam Doo, P. (1985). The Flocculation of Pulp Fibers. In *Transactions of the Eight Fundamental Research Symposium* (pp 265–310).

Kerekes, Richard. (2006). Rhology of fibre suspensions in papermaking : An overview of recent research. *Nordic Pulp & Paper Research Journal, 21*(5), 100-114. https://doi.org/10.3183/NPPRJ-2006-21-05-p598-612

Klemm, D., Kramer, F., Moritz, S., Lindström, T., Ankerfors, M., Gray, D., & Dorris, A. (2011). Nanocelluloses: A new family of nature-based materials. *Angewandte Chemie - International Edition*, *50*(24), 5438–5466. https://doi.org/10.1002/anie.201001273

Koponen, A., & Haavisto, S. (2018). Analysis of industry related flows by optical coherence tomography - a review. *KONA Powder and Particle Journal*. Published online 19 November 2019. https://doi.org/10.14356/kona.2020003

Koponen, A., Lauri, J., Haavisto, S., & Fabritius, T. (2018). Rheological and flocculation analysis of microfibrillated cellulose suspension using optical coherence tomography. *Applied Sciences (Switzerland)*, *8*(5), 755. https://doi.org/10.3390/app8050755

Koponen, A., Haavisto, S., Salmela, J., & Kataja, M. (2019). Slip flow and wall depletion layer of microfibrillated cellulose suspensions in a pipe flow. In *Annual Transactions of the Nordic Society of Rheology, 27,* 13–20.

Kumar, V., Nazari, B., Bousfield, D., & Toivakka, M. (2016). Rheology of microfibrillated cellulose suspensions in pressure-driven flow, *Applied Rheology 26*(4), 43534. https://doi.org/10.3933/APPLRHEOL-26-43534

Kumar, V., Ottesen, V., Syverud, K., Gregersen, Ø., & Toivakka, M. (2017). Coatability of cellulose nanofibril suspensions: Role of rheology and water retention. *BioResources*, *12*(4), 7656–7679. https://doi.org/10.15376/biores.12.4.7656-7679

Lasseuguette, E., Roux, D., & Nishiyama, Y. (2008). Rheological properties of microfibrillar suspension of TEMPO-oxidized pulp. *Cellulose*, *15*(3), 425–433. https://doi.org/10.1007/s10570-007-9184-2

Li, M., Wu, Q., Song, K., Qing, Y., & Wu, Y. (2015). Cellulose nanoparticles as modifiers for rheology and fluid loss in bentonite water-based fluids. *ACS Applied Materials and Interfaces*, *7*(8), 5009–5016. https://doi.org/10.1021/acsami.5b00498

Li, Q., Raj, P., Husain, F., Varanasi, S., Rainey, T., Garnier, G., & Batchelor, W. (2016). Engineering cellulose nanofibre suspensions to control filtration resistance and sheet permeability. *Cellulose*, *23*(1), 391–402. https://doi.org/10.1007/s10570-015-0790-0

Lowys, M., Desbrières, J., & Rinaudo, M. (2001). Rheological characterization of cellulosic microfibril suspensions. Role of polymeric additives. *Food Hydrocolloids*, *15*(1), 25–32. https://doi.org/10.1016/S0268-005X(00)00046-1

Mewis, J., & Wagner, N. (2012). *Colloidal Suspension Rheology*. New York: Cambridge University Press.

Moberg, T., Rigdahl, M., Stading, M., & Bragd, E. (2014). Extensional viscosity of microfibrillated cellulose suspensions. *Carbohydrate Polymers*, *102*(1), 409–412. https://doi.org/10.1016/j.carbpol.2013.11.041

Mohtaschemi, M., Dimic-Misic, K., Puisto, A., Korhonen, M., Thaddeus, M., Paltakari, J., & Alava, M. (2014). Rheological characterization of fibrillated cellulose suspensions via bucket vane viscometer. *Cellulose*, *21*(3), 1305–1312. https://doi.org/10.1007/s10570-014-0235-1

Mohtaschemi, M., Sorvari, A., Puisto, A., Nuopponen, M., Seppälä, J., & Alava, M. (2014). The vane method and kinetic modeling: shear rheology of nanofibrillated cellulose suspensions. *Cellulose*, *21*(6), 3913–3925. https://doi.org/10.1007/s10570-014-0409-x

Mongruel, A., & Cloitre, M. (1999). Shear viscosity of suspensions of aligned non-Brownian fibres. *Rheologica Acta*, *38*(5), 451–457. https://doi.org/10.1007/s003970050196

Mosse, W., Boger, D., & Garnier, G. (2012). Avoiding slip in pulp suspension rheometry. *Journal of Rheology*, *56*(6), 1517–1533. https://doi.org/10.1122/1.4752193

Naderi, A., & Lindström, T. (2014). Carboxymethylated nanofibrillated cellulose: effect of monovalent electrolytes on the rheological properties. *Cellulose 21*(5), 3507–3514. https://doi.org/10.1007/s10570-014-0394-0

Nazari, B., Kumar, V., Bousfield, D., & Toivakka, M. (2016). Rheology of cellulose nanofibers suspensions: Boundary driven flow. *Journal of Rheology*, *60*(6), 1151–1159. https://doi.org/10.1122/1.4960336

Nechyporchuk, O., Belgacem, M., & Bras, J. (2016). Production of cellulose nanofibrils: A review of recent advances. *Industrial Crops and Products*, *93*, 2–25. https://doi.org/10.1016/j.indcrop.2016.02.016

Nechyporchuk, O., Belgacem, M., & Pignon, F. (2014). Rheological properties of micro-/nanofibrillated cellulose suspensions: Wall-slip and shear banding phenomena. *Carbohydrate Polymers*, *112*, 432–439. https://doi.org/10.1016/j.carbpol.2014.05.092

Pääkkö, M., Ankerfors, M., Kosonen, H., Nykänen, A., Ahola, S., Österberg, M., Ruokolainen, J., Laine, J., Larsson, P., Ikkala, O. & Lindström, T. (2007). Enzymatic hydrolysis combined with mechanical shearing and high-pressure homogenization for nanoscale cellulose fibrils and strong gels. *Biomacromolecules*, *8*(6), 1934–1941. https://doi.org/10.1021/bm061215p

Pääkkönen, T., Dimic-Misic, K., Orelma, H., Pönni, R., Vuorinen, T., & Maloney, T. (2016). Effect of xylan in hardwood pulp on the reaction rate of TEMPO-mediated oxidation and the rheology of the final nanofibrillated cellulose gel. *Cellulose*, *23*(1), 277–293. https://doi.org/10.1007/s10570-015-0824-7

Petrich, M., Koch, D., & Cohen, C. (2000). Experimental determination of the stress-microstructure relationship in semi-concentrated fiber suspension*s. Journal of Non-Newtonian Fluid Mechanics, 95*(2-3). 101-133. https://doi.org/10.1016/S0377-0257(00)00172-5

Quennouz, N., Hashmi, S., Choi, H., Kim, J., & Osuji, C. (2016). Rheology of cellulose nanofibrils in the presence of surfactants. *Soft Matter*, *12*(1), 157–164.

https://doi.org/10.1039/c5sm01803j

Raj, P., Blanco, A., de la Fuente, E., Batchelor, W., Negro, C., & Garnier, G. (2017). Microfibrilated cellulose as a model for soft colloid flocculation with polyelectrolytes. *Colloids and Surfaces A: Physicochemical and Engineering Aspects*, *516*, 325–335. https://doi.org/10.1016/j.colsurfa.2016.12.055

Raj, P., Mayahi, A., Lahtinen, P., Varanasi, S., Garnier, G., Martin, D., & Batchelor, W. (2016). Gel point as a measure of cellulose nanofibre quality and feedstock development with mechanical energy. *Cellulose*, *23*(5), 3051–3064. https://doi.org/10.1007/s10570-016-1039-2

Saarikoski, E., Rissanen, M., & Seppälä, J. (2015). Effect of rheological properties of dissolved cellulose/microfibrillated cellulose blend suspensions on film forming. *Carbohydrate Polymers*, *119*, 62–70. https://doi.org/10.1016/j.carbpol.2014.11.033

Saarikoski, E., Saarinen, T., Salmela, J., & Seppälä, J. (2012). Flocculated flow of microfibrillated cellulose water suspensions: An imaging approach for characterisation of rheological behaviour. *Cellulose*, *19*(3), 647–659. https://doi.org/10.1007/s10570-012-9661-0

Saarinen, T., Haavisto, S., Sorvari, A., Salmela, J., & Seppälä, J. (2014). The effect of wall depletion on the rheology of microfibrillated cellulose water suspensions by optical coherence tomography. *Cellulose*, *21*(3), 1261–1275. https://doi.org/10.1007/s10570-014-0187-5

Schenker, M, Schoelkopf, J., Gane, P., & Mangin, P. (2018). Influence of shear rheometer measurement systems on the rheological properties of microfibrillated cellulose (MFC) suspensions. *Cellulose*, *25*(2), 961–976. https://doi.org/10.1007/s10570-017-1642-x

Schenker, M., Schoelkopf, J., Gane, P., & Mangin, P. (2019). Rheology of microfibrillated cellulose (MFC) suspensions: influence of the degree of fibrillation and residual fibre content on flow and viscoelastic properties. *Cellulose*, *26*(2), 845–860. https://doi.org/10.1007/s10570-018-2117-4

Shao, Y., Chaussy, D., Grosseau, P., & Beneventi, D. (2015). Use of microfibrillated cellulose/lignosulfonate blends as carbon precursors: impact of hydrogel rheology on 3D printing. *Industrial and Engineering Chemistry Research*, *54*(43), 10575–10582. https://doi.org/10.1021/acs.iecr.5b02763

Sumida, M. (2013). Flow Properties of Wood Pulp Suspensions in Pipes. *World Academy of*

Science, Engineering and Technology, International Journal of Mechanical, Aerospace, Industrial, Mechatronic and Manufacturing Engineering, 7(11), 2202–2206.

Switzer, L. H., & Klingenberg, D. J. (2003). Rheology of sheared flexible fiber suspensions via fiber-level simulations. *Journal of Rheology*, *47*(3), 759–778. https://doi.org/10.1122/1.1566034

Tatsumi, D., Ishioka, S., & Matsumoto, T. (2002). Effect of fiber concentration and axial ratio on the rheological properties of cellulose fiber suspensions. *Nihon Reoroji Gakkaishi*, *30*(1), 27–32. https://doi.org/10.1678/rheology.30.27

Turpeinen, T., Jäsberg, A., Haavisto, S., Liukkonen, J., Salmela, J., & Koponen, A. (2019). Pipe rheology of microfibrillated cellulose suspensions. *Cellulose*, accepted.

Vadodaria, S., Onyianta, A., & Sun, D. (2018). High-shear rate rheometry of micro-nanofibrillated cellulose (CMF/CNF) suspensions using rotational rheometer. *Cellulose*, *25*(10), 5535–5552. https://doi.org/10.1007/s10570-018-1963-4

Varanasi, S., He, R., & Batchelor, W. (2013). Estimation of cellulose nanofibre aspect ratio from measurements of fibre suspension gel point. *Cellulose*, *20*(4), 1885–1896. https://doi.org/10.1007/s10570-013-9972-9

Wagner, J., Mount, E., & Giles, H. (2014). *Extrusion* (2nd edition). William Andrew, Incorporated.

Winuprasith, T., & Suphantharika, M. (2013). Microfibrillated cellulose from mangosteen (Garcinia mangostana L.) rind: Preparation, characterization, and evaluation as an emulsion stabilizer. *Food Hydrocolloids*, *32*(2), 383–394. https://doi.org/10.1016/j.foodhyd.2013.01.023

Wågberg, L., Decher, G., Norgren, M., Lindström, T., Ankerfors, M., & Axnäs, K. (2008). The build-up of polyelectrolyte multilayers of microfibrillated cellulose and cationic polyelectrolytes. *Langmuir*, *24*(3), 784–795. https://doi.org/10.1021/la702481v